MASTER

THE MECHANISTIC PREDICTION OF FISSION-GAS BEHAVIOR DURING IN-CELL TRANSIENT HEATING TESTS ON LWR FUEL USING THE GRASS-SST AND FASTGRASS COMPUTER CODES

by

J. Rest and S. M. Gehl

Prepared for

5th SMiRT Conference

Berlin, Germany

August 13-17, 1979

U of C-AUA-USDOE

ARGONNE NATIONAL LABORATORY, ARGONNE, ILLINOIS

Operated under Contract W-31-109-Eng-38 for the U. S. DEPARTMENT OF ENERGY

SUMMARY

GRASS SST and FASTGRASS are mechanistic computer codes for predicting fission gas behavior in UO_2 base fuels during steady state and transient conditions. FASTGRASS was developed in order to satisfy the need for a fast-running alternative to GRASS SST. Although based on GRASS SST, FASTGRASS is approximately an order of magnitude quicker in execution. The GRASS SST transient analysis has evolved through comparisons of code predictions with the fission gas release and physical phenomena that occur during reactor operation and transient direct electrical heating (DEH) testing of irradiated light-water reactor fuel. The FASTGRASS calculational procedure is described in this paper, along with models of key physical processes included in both FASTGRASS and GRASS-SST. Predictions of fission gas release obtained from GRASS-SST and FASTGRASS analyses are compared with experimental observations from a series of DEH tests. The major conclusion is that the computer codes should include an improved model for the evolution of the grain-edge porosity.

1. Introduction

GRASS-SST is a comprehensive mechanistic computer code for predicting fission-gas [1]

been verified for steady-power irradiations in the H. B. Robinson Reactor, the [illegible] Virginia Tube Reactor, and the Saxton Reactor and for 11 transient direct-electrical-heati (DEH) tests on irradiated commercial LWR fuel.[1,2] GRASS-SST is currently coupled to the LIFE-LWR fuel-behavior code [1] and the Direct Electrical Heating Transient Temperature Dis bution (DEHITD) code[2] for steady-power and DEH transient calculations, respectively, and [illegible]. GRASS-SST is strongly dependent on the number of nonlinear, coupled integral-partial-differential equations required to obtain a satisfactory solution for the bubble size distr bution functions. Fission gas release and swelling are calculated directly once the gas-bubble distributions have been determined.

For many situations in which detailed knowledge of fission gas bubble size distri butions is not required (e.g., LIFE-LWR and FRAP scoping studies), it is desirable to mini mize computer execution time. In order to retain the comprehensive calculational capabilit of GRASS SST while at the same time providing a fast-running option to GRASS-SST, the devel ment of the FASTGRASS code was initiated. Although based on GRASS-SST, FASTGRASS is approx mately an order of magnitude faster in execution.

The FASTGRASS calculational procedure is described in this paper, along with model of key physical processes included in both FASTGRASS and GRASS-SST. A comprehensive treat ment of GRASS-SST has been published elsewhere[1] and is not included here. Predictions of fission-gas release obtained from GRASS-SST and FASTGRASS analyses are compared with experi mental observation for a series of DEH tests. The discussion of these results emphasizes the need for the computer codes to include an improved model for the evolution of the grain edge porosity.

2. FASTGRASS Calculational Procedure

The most important differences between FASTGRASS and GRASS SST are in the algorith used for calculating the evolution of bubble density and size over time. In GRASS-SST, th bubble-size distribution is specified by calculating the densities of bubbles in each of a number of bubble-size classes. Each bubble-size class is characterized by an average numbe of atoms per bubble, the value of which differs from that of the preceding size class by a constant multiplier. (The number of size classes is a variable that is determined dynamic-ally during a computer run.) Changes in the bubble-size distribution, caused by bubble coalescence and re-solution, for example, are determined by solving a large number of integral-differential equations for each time step. Solutions are carried out for bubbles on grain surfaces, along dislocations, and in the bulk matrix.[1] The iterative solution of a large number of coupled equations is a major contributor to the computer run times of GRASS SST.

In contrast to the multiclass description of the bubble-size distribution in GRASS-SST, FASTGRASS uses only two classes: one for single gas atoms and one for gas bubbl. In addition, the description of bubbles on dislocations has been deleted. In GRASS-SST, t [illegible] intergranular, intragranular, and dis[illegible].

classes are available to fully characterize the distributions. In FASTGRASS, with only two size classes available for inter- and intragranular bubbles, separate descriptions of the

atoms are characterized by their number density and atomic radius, while the gas bubbles are characterized by number density and average size, expressed as the number of atoms per bubble. The number densities of atoms and bubbles are determined for both the intragranular and grain-surface regions by solving the following set of equations:

$$\frac{df_1}{dt} = -a_1 f_1^2 - b_1 f_1 + c_1, \tag{1}$$

$$\frac{df_2}{dt} = -b_2 f_2 + c_2, \tag{2}$$

$$\frac{dg_1}{dt} = -A_1 g_1^2 - B_1 g_1 + C_1, \tag{3}$$

and

$$\frac{dg_2}{dt} = -B_2 g_2 + C_2, \tag{4}$$

where f_1 and f_2 are the single-atom and bubble densities, respectively, for the intragranular region, and g_1 and g_2 are the corresponding quantities for the grain boundaries. The other parameters are defined as follows:

a_1, A_1: Rate, in cm^3/s, at which intra- and intergranular gas atoms, respectively, are lost due to nucleation into gas bubbles.

b_1: Rate, in s^{-1}, at which intragranular gas atoms are lost due to diffusion to gas bubbles and biased migration to grain boundaries.

c_1: Difference between (1) the rate, in atoms $cm^{-3}s^{-1}$, at which intragranular gas atoms are generated by fissioning and re-solution and (2) the rate at which the gas atoms are lost by random diffusion to grain boundaries. For transient calculations, the loss of gas atoms due to random diffusion to grain boundaries is not included in c_1, but is included along with the biased diffusion component in b_1.

b_2: Rate, in s^{-1}, at which intragranular bubbles are lost by biased migration to grain boundaries and re-solution.

c_2: Rate, in atoms $cm^{-3}s^{-1}$, at which intragranular bubbles are produced by nucleation and diffusion of gas atoms to bubbles.

B_1: Rate, in s^{-1}, at which intergranular gas atoms are lost by diffusion to bubbles, migration out of the annulus, migration to the grain edges, and re-solution.

C_1: Rate, in atoms $cm^{-3}s^{-1}$, at which intergranular gas atoms are produced by diffusion of atoms from the lattice, migration of atoms into the annulus (up the temperature gradient) from the bordering annulus, and re-solution.

B_2: Rate, in s^{-1}, at which intergranular bubbles are lost by biased migration out of the annulus, biased migration to grain edges, and re-solution.

C_2: Rate, in atoms $cm^{-3}s^{-1}$, at which intergranular gas bubbles are produced by

nucleation, diffusion of gas atoms to bubbles, migration of bubbles from the [illegible] into the annulus (up the temperature gradient) [illegible].

The above parameters are, in general, functions of the average bubble size, S, which is determined as follows: During each time step, the processes of bubble nucleation, gas-atom diffusion to bubbles, bubble coalescence, and bubble re-solution can lead to changes in the average bubble size. Coalescence increases S, while re-solution decreases S; bubble nucleation and gas-atom diffusion to bubbles tend to stabilize S. Let ξ be the fractional change in bubble density during a particular time step. Then

$$\xi = \frac{Fh}{\gamma_2} \tag{4}$$

where F is the rate at which the bubble density is changing as a result of the above-mentioned processes, $\gamma_2 = f_2$ or g_2 is the bubble density, and h is the internal time step of the code. If ξ is greater than a threshold value ε and bubble density is increasing, the bubble size is increased by a factor of δ. Similarly, if ξ is greater than ε and bubble density is decreasing, the average bubble size is decreased by a factor of δ. Note that a change in bubble size leads to a corresponding change in bubble density, since the total number of gas atoms in bubbles is conserved. The convergence parameters ε and δ were determined to have the values 0.05 and 5, respectively, by decreasing them to the point where further reductions had a minimal effect on calculated results.

3. Models Describing Fission-Gas Phenomena During Transient Heating Conditions

Comparisions of GRASS-SST predictions of gas release and bubble-size distributions with the results of DEH transient tests have resulted in the development and inclusion in GRASS-SST and, subsequently, FASTGRASS of the following key models:

3.1 Gas-channel Formation on Grain Surfaces

SEM examination of DEH-tested fuel[2] has revealed the development of sinuous channels on the grain faces after a saturation density of grain-boundary fission gas has been attained (i.e., after a specific fraction of the grain surface has been occupied by gas bubbles). These face channels link up and extend to the grain-edge channels, thus enhancing the release of gas from the grain surfaces.

The fraction of the grain surface occupied by gas bubbles can be calculated directly from the fission-gas bubble distribution, as follows:

If r_i is the average radius of grain boundary bubbles in the *ith* size class, and g_i is the volume density of such bubbles, then the projected areal coverage per unit volume, A_i, of these bubbles on the boundary is given by

$$A_i = \pi r_i^2 g_i. \tag{6}$$

Eq. (6) assumes spherical bubbles whereas lenticular shapes might be expected as a result of grain-boundary tension effects. However, SEM examinations[2] of the DEH-tested fuel reveal that the grain-boundary bubbles, on the average, do not deform appreciably from sphericity.

The total projected coverage per unit volume, A, of grain-boundary bubbles (gas atoms included, i.e., $i = 1$) is then simply

$$\sum_{i=1}^{N} \quad \sum_{i=1}^{N} \qquad (7)$$

If the gas is assumed to occupy equal, close-packed, touching bubbles, then the maximum areal coverage per unit area of grain boundary is A* = 0.907. (Under conditions where this assumption is not valid, A* <0.907. The calculated results are relatively insensitive to values of A* $\geq$0.50.) Grain-boundary saturation (i.e., the initiation of gas-channel interconnection) occurs when

$$A \geq A^* S_v^{\alpha\alpha}, \qquad (8)$$

Where $S_v^{\alpha\alpha}$ is the grain-boundary area per unit volume.

When eq. (8) is satisfied a portion of the grain-boundary gas is vented to the grain edges. Subsequently, if

$$A < A^* S_v^{\alpha\alpha},$$

the channels are assumed to sinter shut and remain so until eq. (8) is again satisfied.

3.2 Edge-tunnel Interlinkage

SEM examinations of DEH-tested fuel[2] have also revealed the development of interconnected tunnels of gas along the grain edges. Recent experimental evidence suggests that the establishment of these interconnected edge tunnels is necessary for transient gas release during DEH tests.

In the GRASS treatment of interlinked porosity, which is statistical in nature, the degree of pore interlinkage along the grain edges is a function of both the grain and pore-size distributions. The model[1], which is based on the mathematical theory of percolation, uses the concept of an arbitrary distribution of sites with randomly distributed bonds or links that join pairs of sites.

In contrast to the experimental results described in Refs. [1] and [2], the above formalism for calculating the evolution of interconnected porosity does not predict that a rapid increase in long-range porosity interconnection will occur after a critical value of swelling due to fission-gas bubbles has been reached. The probable reasons for this deficiency are as follows: (a) The geometry assumed in the above model does not correspond to observations of DEH- and PBF-tested fuel. (b) GRASS does not include a realistic calculation of the size distribution of pores in which the internal gas pressure is less than the surface tension-induced pressure. (c) Material properties used in the GRASS calculation of the pore-size distribution are experimentally almost inaccessible.

Thus, to provide a more realistic calculation of the pore-interlinkage fraction, the statistical model is supplemented by the additional criterion

$$\text{pore-interlinkage fraction} = 1.0, \text{ if } B_{v(edge)} > B_{v(crit)}, \qquad (9)$$

where $B_{v(edge)}$ is the calculated volume strain due to grain-edge fission-gas bubbles, and $B_{v(crit)} = 0.05$ is the critical gas-bubble volume fraction above which extensive long-range interconnection of the grain-edge tunnels is assumed to take place. When eq. (9) is satisfied, all the grain-edge gas in the fuel node under consideration is released to the

exterior of the fuel. If, subsequently, $B_{v(edge)}$ becomes less than $B_{v(crit)}$, the edge tunnels are assumed to sinter shut, and the calculation of pore interlinkage is again performed via [illegible] theory. [illegible] and Tucker[3] observed that, in [illegible] UO_2, interlinked grain edge [illegible] when the volume fraction was [illegible]. The critical value for tunnel interlinkage in GRASS is taken from their work.

3.3 Effect of Transient Heating on the Mobility of Intragranular Fission-gas Bubbles

Analyses with GRASS-SST[1] for steady-state conditions, coupled with experimentally determined fission-gas release during DEH tests, indicate that large quantities of gas are being transported out of the UO_2 grains during transient heating. This release of fission gas from the grains is much greater than can be explained by means of empirical steady-state diffusivities measured under isothermal annealing conditions[1]. Steady-state, in-pile calculations are complicated by the interplay of bubble diffusivities and re-solution rate. The validity of using empirical steady-state diffusivities having values much lower than predicted by a surface-diffusion mechanism is dependent on the validity of the re-solution parameter used in the calculations. The value of the re-solution parameter used in the GRASS calculations yields a re-solution rate of $\sim 10^{-6}$/s for a fission rate of 10^{13} fissions/cm$^3\cdot$s. This value is within the range of reported results[1]. In addition, analyses for transient-heating conditions indicate that GRASS SST can account for the rapid diffusion of fission gas out of the UO_2 grains during DEH tests *if the high-temperature bubble mobilities are enhanced due to an increased rate of atom attachment* to and detachment from the bubble surface.

The physical basis behind this approach is as follows. During equilibrium conditions, the bubbles may be faceted, and the rate of motion of a faceted bubble is determined by the frequency of nucleation of steps instead of the time required for atoms to move from a step on one side of a bubble to a step on the other side. (That is, the atom attachment and detachment rate is slower than predicted by surface diffusion.) However, if the atom attachment and the detachment rate increases during transient conditions, higher bubble diffusivities would result.

Since plastic deformation of the UO_2 due to an overpressurized bubble is expected to result in a high density of dislocations around the bubble surface, the diffusivity of such a bubble would be expected to increase rapidly. In effect, bubble diffusion would depend more on the time required for atoms to move from a step on one side of a bubble to a step on the other (i.e., surface diffusion) than on the frequency of nucleation of steps.

The model[1] for the diffusion of overpressurized fission gas bubbles is characterized by the equation

$$D_i = \frac{6.732 \times 10^{-11} \exp\left[-(91{,}000 + 17{,}000\alpha_i)/kT\right]}{(4084 r_i)^{1.62 + 2.38\alpha_i}} \quad (10)$$

where D_i is the diffusivity of a bubble of radius r_i, T is the absolute temperature, k is Boltzmann's constant, and α_i ($\alpha_i \leq 1$) characterizes the degree of nonequilibrium in the lattice surrounding a bubble of radius r_i; the larger α_i becomes, the further the system is from an equilibrium configuration. The expression used for α_i is given by

$$\alpha_i = 1.0 - \exp\cdot(-\tau_i^B/\tau_i^y). \quad (11)$$

In eq. (11),

$$\tau_i^y = \left\{ \frac{2\gamma}{r_i} + \frac{2\sigma_y(T)}{3n_i k} - \frac{(4\pi r_i - 3b_v n_i)}{3n_i k} T_1 \right\} \Big/ \frac{dT}{dt} \qquad (11)$$

where τ_i^y is the time required for a bubble with radius r_i, which contains n_i gas atoms, to obtain an excess pressure sufficient to generate an equivalent stress equal to the yield stress, σ_y, of the surrounding matrix; γ is the effective surface tension; T_1 is the temperature at the beginning of the time interval, and dT/dt is the heating rate. The bubble relaxation time τ_i^B in eq. (11) is given by

$$\tau_i^B(T) = \frac{r_i^2}{D_v c_v^e}, \quad T \geq 1500°C;$$
$$\tau_i^B(T) = \tau_i^B(1500°C), \quad T \leq 1500°C \qquad (13)$$

where c_v^e is the fractional equilibrium vacancy concentration, given by

$$c_v^e = \exp(-E_v^f/kT), \qquad (14)$$

and D_v is the vacancy diffusion coefficient, given by

$$D_v = D_v^o \exp(-E_v^m/kT), \qquad (15)$$

E_v^f and E_v^m are the vacancy formation and migration energies, respectively, and D_v^o is a preexponential factor.

When $\alpha_i \to 0$, eq. (10) approaches the expression[11] for bubble diffusivities based on the isothermal results of Cornell and Gulden. When $\alpha_i \to 1$, eq. (10) approaches the expression for bubble diffusivities based on the theory of surface diffusion. For intermediate values of α_i, the diffusivities given by eq. (10) lie between those given by the empirical expression (as a lower limit) and those obtained from the theory of surface diffusion (as an upper limit).

Eq. (10) is unique in the sense that it relates the bubble diffusivities to the fuel yield stress, heating rate, and vacancy mobility, as well as to fuel temperature and bubble radius. The validity of eq. (10) has been supported by the GRASS-SST and FASTGRASS prediction of transient gas release under a wide range of DEH test conditions (see Section

3.4 Rate of Growth of Coalescing Bubbles During Transient Conditions

During steady-state conditions, it is reasonable to assume that, when two fission-gas bubbles coalesce, the (noninstantaneous) growth of the resultant bubble to equilibrium size can be treated as instantaneous. However, in a transient analysis, this assumption breaks down, and the noninstantaneous growth of coalescing bubbles must be included. The need for a GRASS model that describes the limited growth rate of coalescing bubbles became apparent when GRASS-SST-calculated bubble-size distributions for DEH test conditions were compared with qualitative experimental observations. The code predicted similar end-of-test bubble distributions in the lattice and on the grain boundaries. However, the observed intragranular bubble densities were much lower than predicted.

The effect on the GRASS calculation of a limited rate of growth of coalescing bubbles is a reduction in the rate at which bubbles grow by the amount

$$1.0 - \exp\left(-\tau_i^Y/\tau_i^B\right), \tag{16}$$

where τ_i^Y and τ_i^B are [illegible] (11) and (13), respectively.

4. The Calculation of Transient Temperature Histories

During each time step, GRASS-SST and FASTGRASS accept as input the radial distribution of fuel temperatures. For steady-state irradiation, the temperatures are supplied by an integral fuel-rod code such as LIFE-LWR. For the out-of-reactor DEH tests, temperatures are supplied by the DEHTTD code[2]. This code uses measured values of DEH power input and surface temperature to solve the transient heat-flow equation. Expressions for the thermal and electrical conductivities of irradiated fuel are required in the code; these are taken from the available literature on the properties of UO_2. Some of the problems associated with the use of data obtained from relatively high-purity UO_2 to describe the behavior of irradiated fuel have been described elsewhere[2]. An additional problem is the continual reduction in thermal conductivity caused by fuel microcracking during transient heating. This phenomenon has also been observed during nuclear heating[4]. Failure to account for the reduced thermal conductivity can lead to errors of as much as 600°C in the calculated fuel-center temperatures.

Several models have been developed to describe the effect of fuel microcracking on thermal conductivity[1]. The current model, which was used for the calculations reported in this paper, is based on the assumption of a simple linear relationship between the surface area of microtracks and the reduction of thermal conductivity. Surface area was selected because it gives a convenient measure of the extent of microcracking. Microcracking is assumed to occur linearly with time during the transient until maximum power is reached, after which no additional microcracking is assumed. The formula used to calculate the effective thermal conductivity is

$$T_k' = (1 - aS_v)\, T_k, \tag{17}$$

where T_k is an appropriate literature value for UO_2 thermal conductivity, S_v is the surface area of microcracks per unit volume of structure, a is a time-dependent parameter, and T_k' is the modified thermal conductivity used in the DEHTTD calculations.

The parameter a is used to describe the time-dependent formation of microcracks. The value of a is zero at the start of transient heating, increases linearly with time to a maximum at the time of maximum DEH power, and remains constant thereafter. The maximum value of a was determined by trial-and-error matching of the calculated radius of melting to the experimentally observed value for DEH test 33. The same maximum value of a was used in the temperature calculations for all of the DEH tests.

The surface area of microcracks is generally observed to be a function of radial position in the fuel pellet. Surface area is usually highest at the pellet centerline (or near the edge of the melt zone for tests in which melting occurs) and decreases as the periphery of the pellet is approached. As part of the posttest examination of fuel specimens, the radial profile of microcracking is characterized by measuring S_v in 4 to 6 annular zones. For the purposes of the DEHTTD calculations, the measured values of S_v are approximated by a polynomial, which is substituted into eq. (17) at each radial node of DEHTTD.

5. Comparison of Code Predictions for Transient Gas Release with Experimental Results

series of DEH experiments. FASTGRASS executed these problems approximately one order of magnitude faster than GRASS-SST. The results of these calculations are shown in Figs. 1 and 2. In each of these figures, the solid line indicates the position of perfect agreement between predictions and experiment. As is evident, the GRASS-SST and FASTGRASS predictions are in reasonable agreement with the experimental measurements.

The fact that GRASS-SST and FASTGRASS can predict the DEH transient gas release reasonably well for all DEH tests supports the models of key processes described in Section 3. For example, the mobility of fission-gas bubbles is enhanced during severe nonequilibrium conditions. Using empirical diffusivities measured under isothermal conditions, the code significantly underpredicts the data for transient gas release.

Figure 3 shows GRASS-SST results for the radial profile of transient fission-gas (xenon) release during DEH test 33, plotted with laser-sampling data for krypton. (The FASTGRASS predictions are similar) The predicted results show a gradual decrease in fission-gas release from 96% at a fractional radius of 0.16 to about 90% at a fractional radius of 0.69. The predicted release then sharply decreases in a stepwise manner to about 4% for the rest of the radius. This behavior is in contrast with the relatively smooth decline in the fractional fission-gas release from 82% at a fractional radius of 0.48 to 20 at a fractional radius of 0.90, as shown in Fig. 3. The area under the predicted curve is approximately equal to the area under the experimental curve; this result is reflected in the reasonable GRASS-SST prediction of total transient fission-gas release (~40%) during test 33 as shown in Fig. 1.

6. Discussion of Results

Figures 1 and 2 show that both GRASS-SST and FASTGRASS give reasonable predictions of fission-gas release for a series of DEH experiments that encompass a wide range of heating rates and maximum fuel temperatures. Note that the predictions agree to within a factor of two with the experimental values, and that the predictive capabilities of GRASS-SST and FASTGRASS are roughly equal. Therefore, the greater computing speed of FASTGRASS makes this code an attractive alternative for some analytical descriptions of fuel-rod behavior. On the other hand, GRASS-SST is useful for applications in which more detailed predictions, e.g., bubble-size distributions, are necessary, and for substantiating FASTGRASS predictions for specific conditions of interest.

The differences between the predicted and measured fission-gas release values in Figs. 1 and 2 are the summation of several contributing effects. The following discussion of possible sources of error is not meant to be exhaustive. Rather, the intent is to illustrate some of the problems that have been encountered in using the GRASS-SST and FASTGRASS models.

Inaccuracies in the measurement of the fission gas released during the DEH transient lead to an uncertainty of up to 5% in the reported values[2]. These uncertainties are indicated in Figs. 1 and 2. Uncertainties in the calculated transient temperatures used by GRASS-SST and FASTGRASS can lead to additional errors. These uncertainties are due to the

and the experimental error in surface temperature measurement.

Another source of the differences shown in Figs. 1 and 2 is the oversimplified [illegible] described in Section 3.2. This model is based on the assumption that a rapid long-range interconnection of the grain-edge porosity occurs when the grain-edge gas-bubble fractional swelling exceeds 5%. Thus, the stepwise decrease in the predicted release at a fractional radius of 0.69 in Fig. 3 is due to the transition between fuel regions where the gas-bubble swelling was greater than 5% (for fractional radii less than 0.65) to fuel regions where the swelling was less than 5% (for fractional radii greater than 0.65).

The qualitative difference between the predicted and experimental results for the radial profile of transient fission-gas release (and, calculations indicate, some of the deviation of the predicted gas release from the measured results shown in Figs. 1 and 2) indicates that the GRASS model for the rapid, long-range interconnection of grain-edge porosity is too simple to account for the evolution of the grain-edge porosity observed in PBF-tested fuel. A more realistic calculation of the radial profile of transient fission-gas release would have to include models describing the evolution of the intergranular porosity as a function of the gas-bubble distribution, the temperature and heating rate, the fuel microstructure, and the local stresses generated within the fuel pellet. This work is currently in progress.

References

[1] REST, J, "A Comprehensive Mechanistic Model for the Prediction of Fission-gas Behavior in UO_2-base Fuels During Steady-State and Transient Conditions", ANL-78-53 (June, 1978).

[2] GEHL, S. M., SEITZ, M. G., and REST, J., "Fission-Gas Release From Irradiated PWR Fuel During Simulated PCM-Type Accidents: Progress Report", ANL-77-80 (May, 1978).

[3] TURNBULL, J. A. and TUCKER, M. O., "Swelling in UO_2 Under Conditions of Gas Release", Phil. Mag. 30, 47 (1972).

[4] GEHL, S. M., "Comparison of Fission-gas Release and Mechanical Behavior During Transient Nuclear and Electrical Heating of Light-Water-Reactor Fuels", to be published as ANL-78-60.

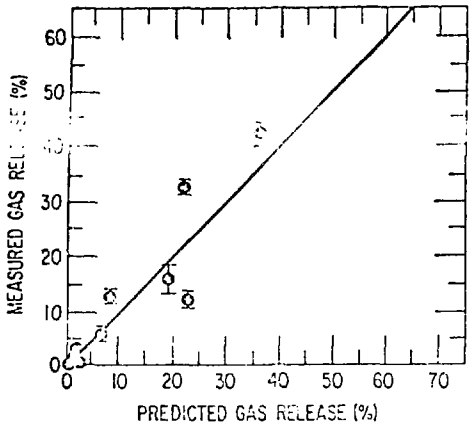

Fig.1 - GRASS–SST–PREDICTED TRANSIENT GAS RELEASE vs EXPERIMENTALLY MEASURED VALUES

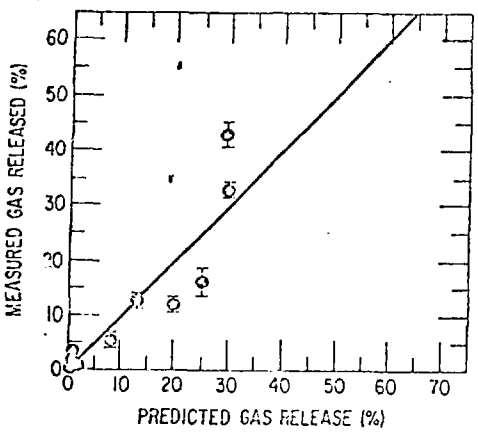

Fig.2 - FASTGRASS–PREDICTED TRANSIENT GAS RELEASE vs EXPERIMENTALLY MEASURED VALUES

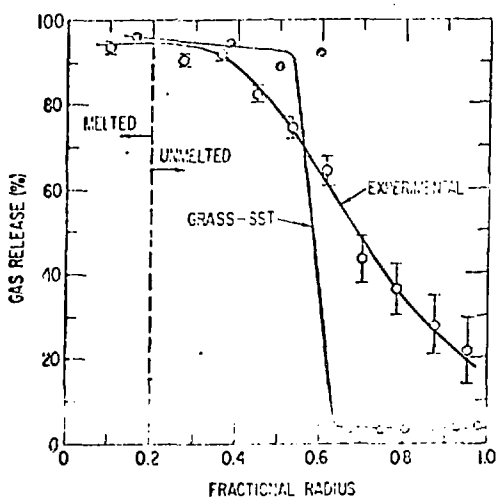

Fig.3 - RADIAL PROFILES OF FISSION-GAS RELEASE FOR DEH TEST 33